Manganese Nitride Complexes in Oxidation States III, IV, and V: Synthesis and Electronic Structure

Henning Kropp,[†,∥] Amanda E. King,[†,∥] Marat M. Khusniyarov,[†] Frank W. Heinemann,[†] Kyle M. Lancaster,[‡] Serena DeBeer,[‡,§] Eckhard Bill,[§] and Karsten Meyer*,[†]

[†]Department of Chemistry and Pharmacy, Inorganic Chemistry, Friedrich-Alexander University of Erlangen-Nuremberg, Egerlandstrasse 1, Erlangen, Germany

[‡]Department of Chemistry and Chemical Biology, Cornell University, Ithaca, New York 14853, United States

[§]Max-Planck-Institute for Chemical Energy Conversion (CEC), Stiftstrasse 34-36, D-45470 Mülheim an der Ruhr, Germany

S Supporting Information

ABSTRACT: The synthesis and characterization of a series of manganese nitrides in a tripodal chelating tris(carbene) ligand framework is described. Photolysis of $[(TIMEN^{xyl})Mn(N_3)]^+$ (where $TIMEN^{xyl}$ = tris[2-(3-xylylimidazol-2-ylidene)ethyl]-amine) yields the isolable molecular Mn^{IV} nitride, $[(TIMEN^{xyl})Mn(N)]^+$. Spectroscopic and DFT studies indicate that this Mn^{IV} d^3 complex has a doublet electronic ground state. The metal-centered one-electron oxidation of this Mn^{IV} species results in formation of the pentavalent Mn^V nitride, $[(TIMEN^{xyl})Mn(N)]^{2+}$. Unlike previously reported, tetragonal Mn^V nitrides with a d^2, nonmagnetic $S = 0$ ground state, this trigonal bipyramidal complex has a triplet ground state $S = 1$. One-electron reduction of $[(TIMEN^{xyl})Mn(N)]^+$ produces the neutral, nonmagnetic trivalent $[(TIMEN^{xyl})Mn(N)]$ species with a d^4 low-spin, $S = 0$, ground state.

There has been renewed interest in high-valent metal nitrides because of their proposed intermediacy in biological and industrial nitrogen fixation processes.[1] Among the most prominent examples of metal nitrides are those of iron[2] and manganese.[3] A number of iron nitride species in both tetragonal and trigonal ligand fields (Figure 1) have been synthesized and characterized both structurally[2a,b] and spectroscopically.[4] In contrast, the majority of structurally characterized manganese nitride complexes adopt either square pyramidal or pseudo-octahedral geometries.[3] The electronic structure of these Mn complexes can be described in terms of the 1+2+1+1 d-orbital splitting of 4-fold symmetrical transition-metal complexes with strong π-donor ligands, studied by Ballhausen and Gray in the classic $[(H_2O)_5V(O)]^{2+}$ cation.[5] However, recent studies by Bendix et al. suggest that the more covalent nitrido ligand (N^{3-}) dominates the ligand field of transition metal complexes to such an extent that the resulting electronic structure approximates linear symmetry.[6] The resulting stabilization of the $d(x^2-y^2)$ orbital leads to a 1+3+1 d-orbital splitting (Figure 1, left), in which the $d(xz)/d(yz)$ set of π^* orbitals is nearly degenerate with the $d(x^2-y^2)$ σ^* orbital; in complexes with weak equatorial donor ligands, the ordering of these orbitals can be reversed.

The majority of reported molecular manganese nitrides to date are in tetragonal ligand fields and have formal +V, +VI, and +VII oxidation states with d^2 low-spin ($S = 0$), d^1 ($S = 1/2$), and d^0 ($S = 0$) ground states, respectively.[3,7] The dearth of tetragonal Mn complexes with terminal nitride (and oxo[8]) ligands in lower oxidation states results from destabilization of the Mn−L multiple bond by population of the strongly antibonding metal-based d-orbitals.

Enforcing a tripodal geometry around a metal center introduces a degeneracy in the metal-based $d(x^2-y^2)$ and $d(xy)$ orbitals (Figure 1, right), thus allowing access to lower-valent metal complexes that feature terminal, multiply bonded ligands. This principle has been demonstrated by Peters et al. in the synthesis of the first Fe^{IV} nitride[4b] as well as Fe^{III} and Fe^{II}
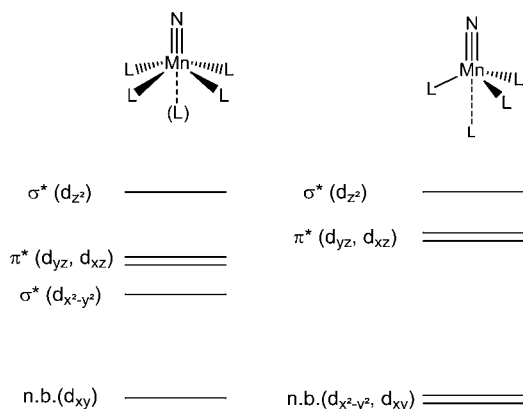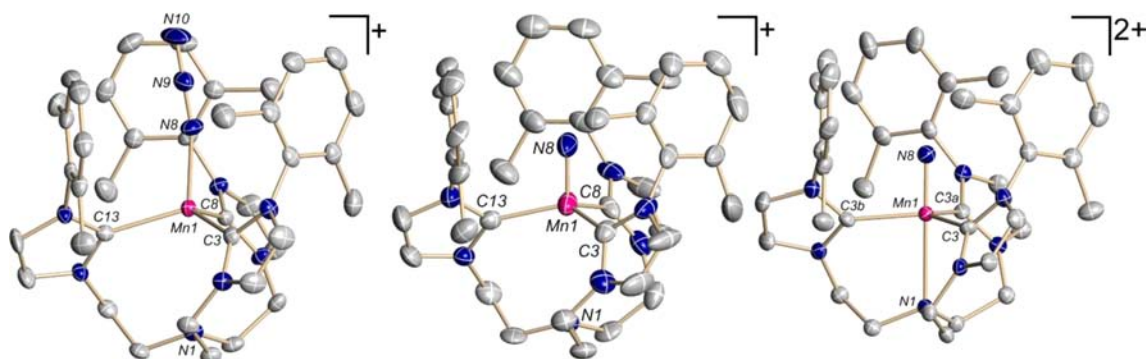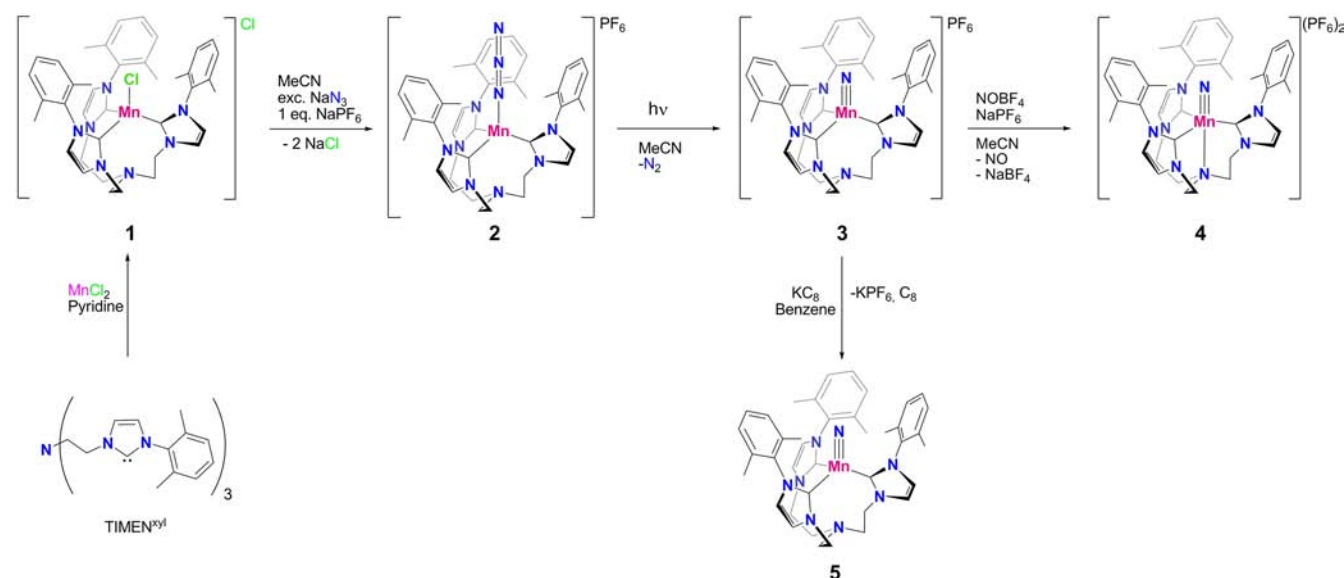

Figure 1. Qualitative d-orbital splitting diagrams for manganese and iron nitride complexes in tetragonal (left) and trigonal (right) ligand fields.

Scheme 1. Synthesis of $[(TIMEN^{xyl})Mn(Cl)]Cl$ (1), $[(TIMEN^{xyl})Mn(N_3)]PF_6$ (2), $[(TIMEN^{xyl})Mn(N)]BPh_4$ (3), $[(TIMEN^{xyl})Mn(N)](PF_6)_2$ (4), and $[(TIMEN^{xyl})Mn(N)]$ (5)


Figure 2. Molecular structures and selected bond lengths (Å) and angles (deg) of **2** (left), **3** (middle), and **4** (right). Solvent molecules, counteranions, and hydrogen atoms are omitted for clarity; thermal ellipsoids are shown at 50% probability. (Left) Molecular structure of **2**: Mn1– N8 2.031(2), N8–N9 1.184(3), N9–N10 1.160(3), Mn1–C3 2.177(3), Mn1–C8 2.184(2), Mn1–C13 2.175(3), Mn1–N8–N9 167.5(2). (Middle) Molecular structure of **3**: Mn1–N8 1.524(3), Mn1–C3 2.102(5), Mn1–C8 1.932(6), Mn1–C13 1.990(5), C3–Mn1–C8 113.8(2), C3– Mn1–C13 117.0(2), C8–Mn1–C13 116.7(2). (Right) Molecular structure of **4**: Mn1–N8 1.546(3), Mn1–C3 2.054(2), Mn1–N1 2.448(3), C– Mn1–C 119.47(2), N8–Mn1–N1 180.

imides.[9] Surprisingly, and to the best of our knowledge, no manganese nitrides in oxidation states +IV or lower have been reported to date. Lu and Peters also were the first to report attempts to synthesize a Mn^{IV} nitride via photolysis and thermolysis of a tris(isopropylphosphino)borate Mn^{II} azide; however, this species could not be isolated, and insight into the electronic structure could only be gained through density functional theory (DFT) calculations.[10] We now report not only the synthesis and characterization of a molecular Mn^{IV} nitride complex, but also expand the series to include the Mn^{V} and Mn^{III} congeners as well.

The syntheses of all disclosed compounds are given in Scheme 1. Addition of 1 equiv of anhydrous manganese(II) chloride to solutions of the tris(carbene) ligand $TIMEN^{xyl}$ in pyridine at room temperature furnishes $[TIMEN^{xyl}Mn(Cl)]Cl$ (**1**) as an analytically pure white solid. Subsequent reaction of **1** with a large excess of sodium azide in the presence of $NaPF_6$ yields $[(TIMEN^{xyl})Mn(N_3)]PF_6$ (**2**). The IR spectrum of **2** shows an intense vibrational band centered at 2094 cm^{-1} that is attributed to the asymmetric azide stretch (Figure S1). Slow

diffusion of ether into acetonitrile solutions of **2** yields single crystals suitable for X-ray diffraction studies. The crystal structure of **2** (Figure 2, left) reveals a slightly angled binding mode of the azide (Mn–N_α–N_β = 167.5°) and a Mn–N_α distance of 2.031(2) Å. The linear coordination of the azide ligand to the Mn^{II} center is the result of the sterically encumbering cylindrical cavity created by the TIMEN ligand framework. This observation is unusual but has been reported for the analogous $[(TIMEN^{mes})Fe(N_3)]^{2+}$ complex.[2a] The amine anchor is 3.137(3) Å away from the metal center, resulting in a four-coordinate Mn^{II} center that is located 0.52 Å above the trigonal plane of the three carbene carbon atoms. Both SQUID magnetometry and EPR spectroscopy establish **2** as a high-spin, d^5 manganese(II) species. Exposure of colorless acetonitrile solutions of **2** to ultraviolet radiation produces deep-red colored solutions of $[(TIMEN^{xyl})Mn(N)]PF_6$ (**3**) with concomitant loss of N_2. The electronic absorption spectrum of **3** exhibits three absorption bands centered at λ = 315, 385, and 488 nm (ε = 6028, 3472, and 1334 M^{-1} cm^{-1}). TD-DFT calculations assign the lowest energy and weakest
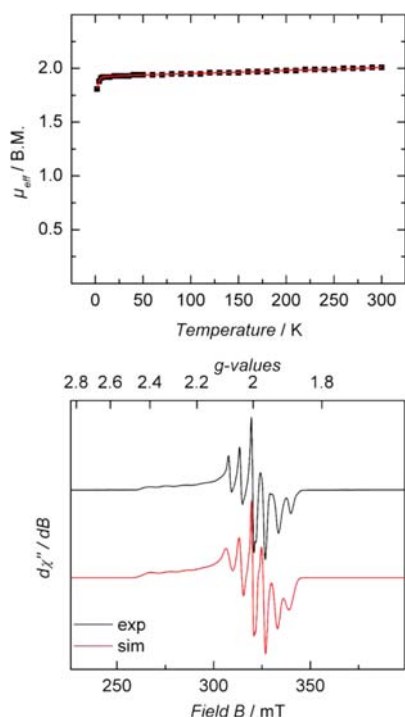
Figure 3. Characterization data for **3**: SQUID magnetization data on a solid sample of **3** (top). Experimental magnetic data are shown in black, and fitted (red line) with $S = 1/2$, $g = 2.06$, superimposed with TIP (159.2×10^{-6} emu) and a minor paramagnetic impurity (1.5%, $S = 5/2$). X-band EPR spectrum of a frozen solution of **3** in 2-methyl THF at 11 K (bottom). Simulation parameters: $g_1 = 1.97$, $g_2 = 1.98$, $g_3 = 2.22$, $A_1 = 77$ MHz, $A_2 = 168$ MHz, $A_3 = 268$ MHz.

transition in the visible part of the spectrum at 488 nm ($\sim$20.500 cm^{-1}) to a predominantly metal-to-ligand charge transfer transition, and the two more intense transitions in the UV are likely ligand-centered (Figures S11–S13). Examination of the IR spectra of **3** and its ^{15}N-labeled isotopomer reveals ν(Mn$\equiv^{14}$N) and ν(Mn$\equiv^{15}$N) stretches at 1033 and 1008 cm^{-1}, respectively; this 25 cm^{-1} shift in stretching frequencies matches the 28 cm^{-1} energy difference predicted by the harmonic oscillator model (Figure S6). The replacement of the PF$_6^-$ anion with BPh$_4^-$ and slow diffusion of ether into a concentrated acetonitrile solution of **3** yields single crystals

suitable for X-ray structure analysis (Figure 2, middle). The short Mn$\equiv$N bond length of 1.524(3) Å is comparable to bond distances seen in other structurally characterized metal nitrides (1.50–1.54 Å).[3] The four-coordinate Mn^{IV} center is located in a trigonal pyramidal ligand environment and resides only 0.42 Å above the trigonal plane of the carbene centers. As expected upon oxidation of Mn^{II} to Mn^{IV}, the distance between the Mn^{IV} center and the nitrogen anchor (N1) shortens to 3.078(3) Å, and the average metal–carbene bond length decreases to 2.008(9) Å. The degenerate electronic ground state (vide infra) is Jahn–Teller active, and thus the crystal structure of **3** also reveals an observable decrease in one of the C–Mn^{IV}–C bond angles and a significantly longer Mn^{IV}–C bond length, resulting in a noticeable deviation from an idealized C_3 geometry.

The electronic structure of **3** was probed using DFT and spectroscopic techniques. Previous DFT studies indicated that a theoretical tris(iso-propylphosphino)borate Mn^{IV} nitride species has a doublet ground state;[10] analogous DFT studies on **3** confirm this predicted preference for the doublet over the quartet state (see Figure 4, middle). The metal-based d-orbitals split into an antibonding set of higher energy, including the d(xz), d(yz), and d(z^2) orbitals and a nonbonding set of lower energy, comprising the d(x^2-y^2) and d(xy) orbitals. A Jahn–Teller distortion removes the degeneracy between the nonbonding {d(x^2-y^2), d(xy)} set and the antibonding d(xz) and d(yz) orbitals, resulting in the observed differences in the Mn^{IV}–C bond lengths and C–Mn^{IV}–C bond angles in the crystal structure of **3** (Figure 2 and Table S4). SQUID magnetometry measurements of **3** provide experimental confirmation of the predicted doublet ground state with a magnetic moment, μ_{eff}, of 2.01 μ_B at 300 K (Figure 3, top). The deviation of the experimental μ_{eff} value from the calculated spin-only value of 1.73 μ_B (with $g_{av} = 2.06$ obtained from the EPR spectrum, vide infra) is most likely due to contributions from a minor high-spin Mn(II) impurity (1.5%).

Electron paramagnetic resonance (EPR) spectroscopy also confirms the doublet ground state for **3** (Figure 3, bottom). The low temperature EPR spectrum of **3** at 11 K exhibits a nearly axial signal that is best simulated with $g_1 = 1.97$, $g_2 = 1.98$, and $g_3 = 2.22$. Hyperfine coupling to the manganese nucleus (^{55}Mn, 100% $I = 5/2$) is evident in the $g_{1,2} \approx 2$ and $g_3 = 2.22$ signals, with $A_{1,2} = 77$ and 168 MHz and $A_3 = 267$ MHz.
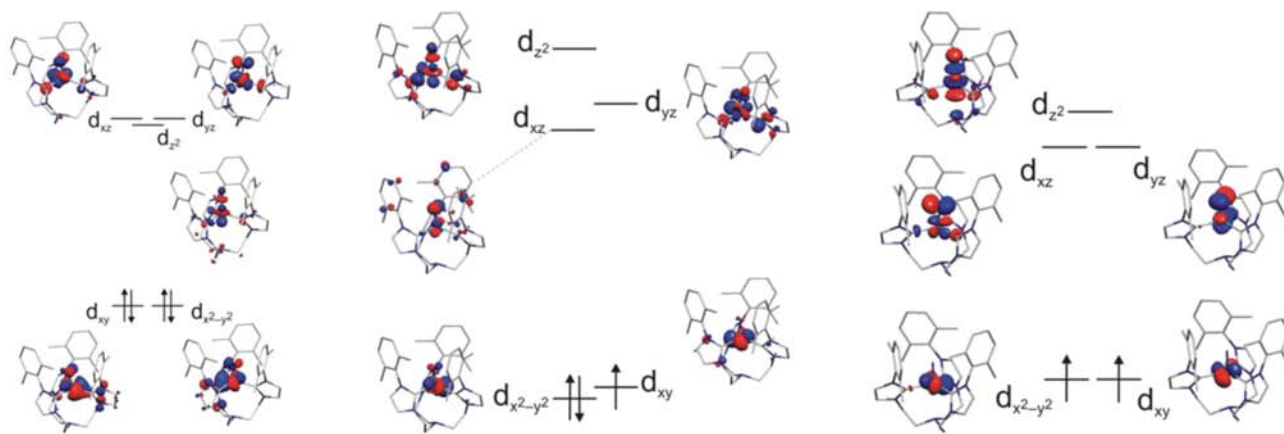
Figure 4. Electronic structure of Mn^{III} nitride **5** (left), Mn^{IV} nitride **3** (middle), and Mn^V nitride **4** (right) as determined by DFT calculations. Frontier Mn-based molecular orbitals of Mn^{III} ($S = 0$), Mn^{IV} ($S = 1/2$), and Mn^V ($S = 1$) were obtained from the spin-unrestricted B3LYP-DFT calculations. Kohn–Sham orbitals (top) and quasi-restricted orbitals (middle, bottom) are shown; the z-axis is parallel to the Mn$\equiv$N vector.

Table 1. Comparison of Bond Lengths (Å) and Angles (deg) in 2, 3, 4, 5, and $[(TIMEN^{xyl})Fe(N)]^+$

|	XRD	EXAFS	DFT
Compound 2			
$M^{II}-C$	2.177(3)	2.15	
	2.184(2)		
	2.175(3)		
$M^{II}-N_\alpha$	2.031(2)	1.96	
$N_\alpha-N_\beta$	1.184(3)		
$N_\beta-N_\gamma$	1.160(3)		
$M^{II}-N_\alpha-N_\beta$	167.5(2)		
Compound 3			
$Mn^{IV}-C$	2.102(5)	2.05	1.988
	1.932(6)		2.018
	1.990(5)		2.023
$M^{IV}-N_{nitride}$	1.524(3)	1.52	1.525
$M^{IV}-N_{anchor}$			3.127
$C-M^{IV}-C$	113.8(2)		109.4
	117.0(2)		110.9
	116.7(2)		127.5
$N-M^{IV}-N$			178.7
Compound 4			
M^V-C	2.054(2)	2.09	2.041
			2.041
			2.042
$M^V-N_{nitride}$	1.546(3)	1.52	1.535
M^V-N_{anchor}	2.448(3)		2.789
$C-M^V-C$	119.47(2)		118.3
$N-M^V-N$	180		180
Compound 5			
$M^{III}-C$		1.95	1.959
$M^{III}-N_{nitride}$		1.59	1.540
$M^{III}-N_{anchor}$			3.435
$C-M^{III}-C$			113.7
			113.9
			114.2
$N-M^{III}-N$			179.9
$\mathbf{[Fe(TIMEN^{xyl})(N)]^{+a}}$			
$M^{IV}-C$	1.956(4)		
$M^{IV}-N_{nitride}$	1.527(3)		
$M^{IV}-N_{anchor}$	2.984(3)		
$C-M^{IV}-C$	114.2(2)		
	119.6(2)		
	115.0(2)		
$N-M^{IV}-N$	178.4(2)		

^{a}From ref 2.

As expected, the electronic structure and spectroscopic properties of the Mn^{IV} nitride **3** are similar to those of the recently reported isoelectronic tris(carbene) Fe^V nitride species, $[PhB(^tBuIm)_3Fe^V \equiv N]BAr_{F24}$ (with $PhB(^tBuIm)_3^-$ = phenyltris(3-*tert*-butylimidazol-2-ylidene)borato, BAr_{F24} = B-$(3,5-(CF_3)_2C_6H_3)_4^-$).[2b]

The electronic configuration shown in Figure 4 (middle) suggests that both the one-electron oxidation and the reduction process should be facile. Accordingly, a cyclic voltammogram of **3** shows two reversible one-electron redox processes at -1.1 and -2.4 V relative to Fc/Fc^+ couple, suggesting straightforward access to both the Mn^V and the Mn^{III} nitrides (Figure S8). Encouraged by these results, we sought the independent syntheses of the Mn^V and Mn^{III} congeners.

Reaction of **3** with 1 equiv of $NOBF_4$ in the presence of 1 equiv of $NaPF_6$ in acetonitrile yields orange solutions of $[(TIMEN^{xyl})Mn(N)](PF_6)_2$ (**4**) with concomitant loss of NO. Slow diffusion of benzene into concentrated acetonitrile solutions of **4** yields crystals suitable for X-ray diffraction analysis. The solid-state structure of **4** (Figure 2, right) differs from that of **3** in several key aspects. Most remarkably, the manganese−nitride bond length increases to 1.546(3) Å upon oxidation from Mn^{IV} to Mn^V, making the $Mn \equiv N$ bond distance in **4** one of the longest bond distances reported for crystallographically characterized terminal Mn^V nitrides.[11] The distance between the highly oxidized manganese ion and the anchoring amine significantly decreases to 2.448(3) Å, and the manganese out-of-plane distance decreases to 0.15 Å, effectively placing the Mn^V center in a trigonal bipyramidal ligand environment.

The complex crystallizes in a C_3 symmetric space group ($P2_13$), rendering all Mn^V-C bonds equivalent at 2.054(2) Å, all $C-Mn^V-C$ bond angles equivalent at 119.47(2)°, and the $N_{nitride}-Mn^V-N_{amine}$ angle to be 180°. All previously published Mn^V nitrides are reported to be nonmagnetic $S = 0$ species.[3] However, complex **4** is best described as an $S = 1$ species on the basis of DFT and spectroscopic studies. Density functional theory calculations replicate the Mn−N nitride, Mn−C bond distances, and C−Mn−C bond angles with high accuracy (Table S2). While the composition of the non- and antibonding orbital sets does not change upon oxidation of **3** to **4**, the nonbonding $d(x^2-y^2)$ and $d(xy)$ orbitals and the antibonding $d(xz)$ and $d(yz)$ orbitals become degenerate. Accordingly, compound **4** is NMR silent. Additionally, the observed effective magnetic moment, μ_{eff}, of 2.87 μ_B at room temperature confirms the triplet ground state of **4** (Figure S14). It is interesting to note that the magnetic moment shows an unusual and pronounced temperature dependency in the range of 2−200 K, which we tentatively assign to intermolecular interaction. An alternative explanation based on strong zero-field splitting or first-order orbital moment can be ruled out because the orbital ground state of the d^2 system in trigonal symmetry is an energetically well-isolated orbital singlet state, which, at most, should experience a weak zero-field splitting. This is well-supported by the quantum chemical calculations (Figure 4, right and Figure S15).

The one-electron reduction of cation **3** to the neutral complex $[(TIMEN^{xyl})Mn(N)]$ (**5**) should furnish a Mn^{III} nitride. This highly unusual, low oxidation state is not yet known for manganese nitride species but is isoelectronic to the recently reported, very stable Fe^{IV} (d^4) nitride species.[2] Accordingly, stirring deep-red suspensions of **3** in benzene over potassium graphite results in dark green solutions of the reduced nitride species **5**. Compound **5** is soluble and stable in nonpolar solvents such as benzene and ether, but is unstable in acetonitrile. Unlike previously reported Fe^{IV} nitride species, **5** is extremely reactive, decomposing at room temperature even in the solid state, and attempts to crystallize **5** have been unsuccessful to date. The diamagnetic NMR spectrum of **5** is similar to that of $[Fe(TIMEN^{xyl})(N)]^+$, displaying the expected 11 resonances between 1.2 and 6.9 ppm (Figure S21). Density functional theory calculations were undertaken to compare the geometry and metrical parameters of **5** with $[(TIMEN^{xyl})Fe-(N)]^+$ (Figure 4, left, and Table 1). The computations indicate that all bond distances are generally longer in the manganese nitride than in the iron nitride; this increase in bond distances is
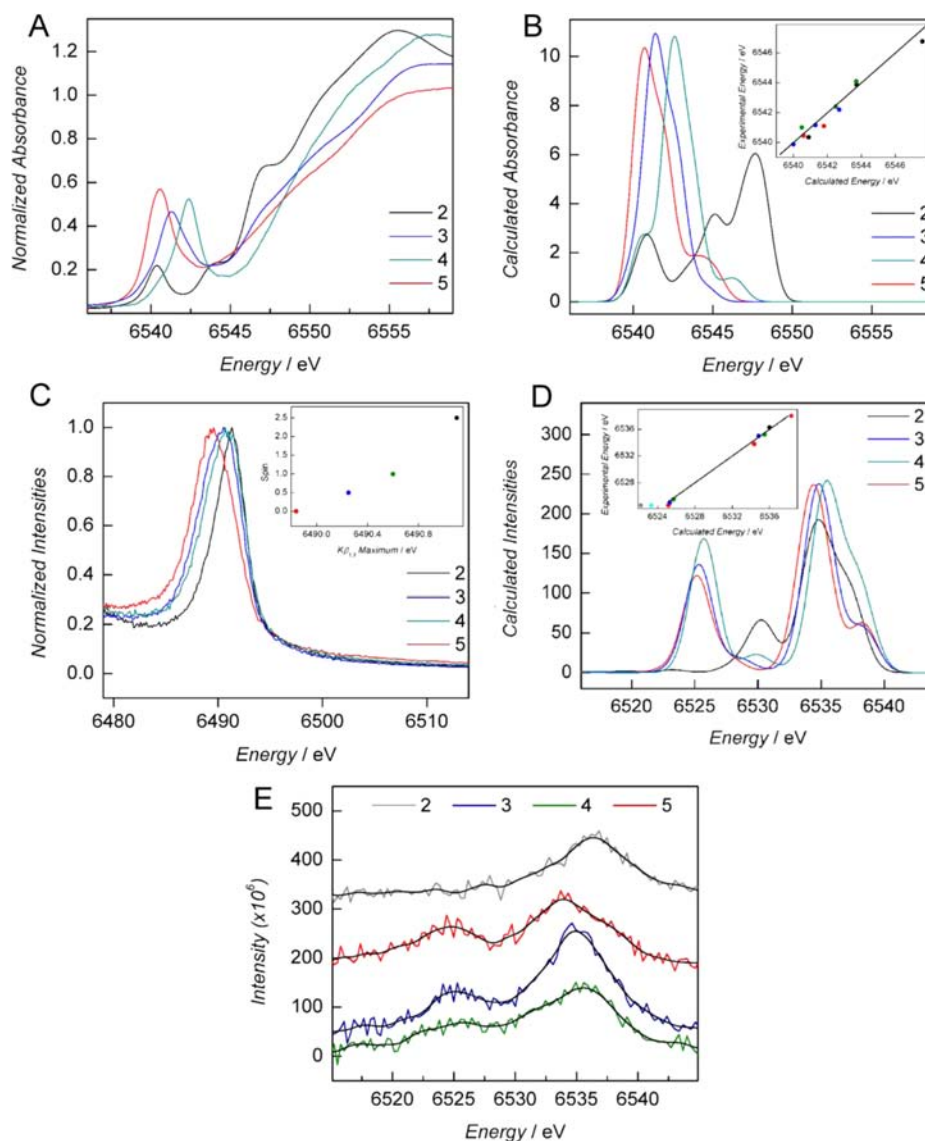
Figure 5. X-ray absorption near edge spectra (XANES, A and B) and X-ray emission (XES) features (C−E) for compounds **2** (black), **3** (blue), **4** (green), **5** (red), **5**-NH (cyan dot), and **5**-NH$_2$ (gray dot). (A) Experimental X-ray absorption near edge spectra. (B) Calculated X-ray absorption near edge spectra and correlation between experimental and shifted calculated XANES pre-edge maxima (inset). (C) Experimental K$\beta_{1,3}$ XES features and correlation between nominal spin and K$\beta_{1,3}$ peak maxima (inset). (D) Calculated V2C XES features and correlation between experimental and calculated V2C peak positions (inset). **5**-NH and **5**-NH$_2$ are indicated by cyan and gray markers, respectively; K$\beta_{2,5}$ features for these molecules are superimposable with those of **5**. (E) V2C XES features. A 60.4 eV scalar energy correction has been applied to all calculated spectra. Uncertainties in experimental band positions in all insets are smaller than the markers.

likely due to the increased nuclear charge of Fe relative to the isoelectronic Mn species.

Mn K-edge X-ray absorption spectra (XAS), including extended X-ray absorption fine structure (EXAFS), were recorded for compounds **2**−**5** to establish physical oxidation states and to afford a consistent series of experimental metrical parameters (Figure 5A). All four compounds display pre-edge absorption features near 6540 eV corresponding to an envelope of transitions dominated in intensity by 1s to 3d excitations. The greater intensities of these features displayed by the nitride complexes **3**−**5** indicate asymmetric coordination,[12] a result of the short formal Mn≡N$_{nitride}$ triple bond. The maxima of these features increase in energy proceeding from **5** to **3** to **4**, indicating incremental increases in physical oxidation state from Mn^{III} to Mn^{IV} to Mn^{V}.[12] Pseudo-Voigt deconvolutions of these pre-edge features reveal a strong correlation between

experimental peak positions and those calculated by TD-DFT (Figure 5B, Table S5).[13] Pre-edge peak areas are calculated to be within 10% of one another, slightly in excess of experimental error. This accords with the experimental pre-edge peak areas, which are identical within 10%. Fitting of the EXAFS from **5** reveals a 1.59 Å M−N scattering path (Figure S26b). DFT geometry optimization of **5** gives a Mn−N bond distance of 1.53 Å. Single and double protonation of the axial nitrogen in **5** (**5**-NH, **5**-NH$_2$) gives calculated Mn−N distances of 1.63 and 1.74 Å, respectively.

Calculated pre-edge features for **5**-NH and **5**-NH$_2$ have approximately 50% peak area relative to **5**. Such differences from **3** and **4** are well in excess of experimental uncertainty due to normalization (Figure S25, Table S5), supporting nitride coordination of **5**.

$K\beta$ X-ray emission spectra (XES) for compounds **2**−**5** are reported in Figure 5C and E. Mn $K\beta$ XES comprise transitions from 3p to a 1s core hole ($K\beta$ main line), as well as transitions to the 1s core hole from occupied ligand-centered molecular orbitals (valence-to-core or V2C).[14] The $K\beta$ main line is split into two components, the $K\beta_{1,3}$ and a lower-energy satellite, $K\beta'$, due primarily to 3p/3d exchange interaction.[14] This latter splitting affords a metric of local spin population at the photoabsorbing Mn.

While the geometry of our experimental setup prohibits measurement of the entire $K\beta'$ feature, the $K\beta_{1,3}$ maximum has been successfully correlated to nominal spin and as such is sufficient for our purposes.[14] From **5** to **3** to **4**, there is an incremental increase in the maximum of the $K\beta_{1,3}$ band in accord with the proposed half-integer spin increase through the series Mn^{III}, Mn^{IV}, and Mn^{V} nitride complexes (Figure 5C). Compound **2**, with its $S = 5/2$ center, appears to highest energy and is slightly removed from linearity with the nitride series, likely due to decreased covalency of the Mn−azide interaction.

The V2C features indirectly probe ligand electronics through the window of the transition metal photoabsorber.[14,15] Manganese V2C spectra are divided into the $K\beta''$ satellite from 6520 to 6530 eV and the $K\beta_{2,5}$ peak from 6530 to 6540 eV. $K\beta''$ features are a result of transitions from ligand-centered ns orbitals, while the $K\beta_{2,5}$ features are transitions from ligand-centered np orbitals. The $K\beta''$ features are highly sensitive to ionization potentials of coordinating atoms, allowing distinction not only by atom type,[1c,16] but also by more subtle perturbations, such as protonation state.[17] As such, V2C XES offers more precise characterization of **5** relative to XAS. Moreover, a simple DFT protocol allows accurate prediction of V2C band positions and intensities.[17] Energies for calculated and experimental V2C spectra for compounds **2**−**5** are in good agreement (Figure 5D). This agreement degrades substantially when considering hypothetically protonated species of **5**, **5**-NH and **5**-NH$_2$, which have $K\beta''$ features shifted to 1 eV lower energy for each successive protonation relative to **5** (Figure S27). Because we could not record the full $K\beta$ XES spectrum for compounds **2**−**5**, the spectra are normalized to the $K\beta_{1,3}$ peak maxima. This prohibits our analysis of peak intensities, although qualitative agreement between experimental and calculated peak intensities is observed across the series.

While not explored experimentally in this report, the reactivity of compounds **3**−**5** is of particular interest. The most well-known example of manganese nitride reactivity is the $Mn^V(N)$ promoted azirindation and amination of olefinic substrates initially developed by Groves and Carreira.[3c,d,18] Extensive spectroscopic studies have established a $S = 0$ spin state of these tetrapodal $Mn^V(N)$ complexes, and the requirement to form the corresponding Mn^V imido complexes using organic anhydrides and acyl chlorides in the absence of other activators prior to N-atom transfer implies that the nitrido moiety has some nucleophilic character. As seen in porphyrinato- and salen Mn nitride complexes, the observed electron spin densities for compounds **3**−**5** are located on the metal and not on the nitrido ligand. Thus, it is anticipated that compounds **3**−**5** would more readily participate in reactions observed for other metal nitridos[19] than reactions typically associated with metal−nitrene (or −oxene) complexes.[20]

In summary, employing the tripodal tris(carbene) ligand framework TIMEN^{xyl} has permitted the synthesis and characterization of a new series of manganese nitrides in the +V, +IV, and +III oxidation states. To the best of our

knowledge, compound **4** also is the first paramagnetic Mn^V nitride reported. Furthermore, compounds **3** and **5** represent the first examples of lower-valent manganese nitrides that have been fully characterized via spectroscopic and computational studies. Additionally, **4** represents the first molecular Mn^V nitride located in a trigonal ligand field. The access to lower-valent manganese nitrides is expected to result in new reactivity, a proposition that we are currently exploring.

■ ASSOCIATED CONTENT

⑤ Supporting Information

Supporting graphics, experimental conditions, synthetic procedures, theoretical calculations, and spectroscopic data. This material is available free of charge via the Internet at http://pubs.acs.org.

■ AUTHOR INFORMATION

Corresponding Author
karsten.meyer@chemie.uni-erlangen.de

Author Contributions
‖These authors contributed equally.

Notes
The authors declare no competing financial interest.

■ ACKNOWLEDGMENTS

■ REFERENCES

(1) (a) Svastits, E. W.; Dawson, J. H.; Breslow, R.; Gellman, S. H. *J. Am. Chem. Soc.* **1985**, *107*, 6427−6428. (b) Ertl, G. *Angew. Chem., Int. Ed. Engl.* **1990**, *29*, 1219−1227. (c) Lancaster, K. M.; Roemelt, M.; Ettenhuber, P.; Hu, Y.; Ribbe, M. W.; Neese, F.; Bergmann, U.; DeBeer, S. *Science* **2011**, *334*, 974−977. (d) Hohenberger, J.; Ray, K.; Meyer, K. *Nat. Commun.* **2012**, *3*, 720. (e) Scepaniak, J. J.; Vogel, C. S.; Khusniyarov, M. M.; Heinemann, F. W.; Meyer, K.; Smith, J. M. *Science* **2011**, *331*, 1049−1052.

(2) (a) Vogel, C.; Heinemann, F. W.; Sutter, J.; Anthon, C.; Meyer, K. *Angew. Chem., Int. Ed.* **2008**, *47*, 2681−2684. (b) Scepaniak, J. J.; Fulton, M. D.; Bontchev, R. P.; Duesler, E. N.; Kirk, M. L.; Smith, J. M. *J. Am. Chem. Soc.* **2008**, *130*, 10515−10517.

(3) Mn nitrides with porphyrin ligands: (a) Hill, C. L.; Hollander, F. J. *J. Am. Chem. Soc.* **1982**, *104*, 7318−7319. (b) Buchler, J. W.; Dreher, C.; Lay, K. L.; Lee, Y. J.; Scheidt, W. R. *Inorg. Chem.* **1983**, *22*, 888−891. Mn nitrides with salen-type ligands: (c) Du Bois, J.; Hong, J.; Carreira, E. M.; Day, M. W. *J. Am. Chem. Soc.* **1996**, *118*, 915−916. (d) Du Bois, J.; Tomooka, C. T.; Hong, J.; Carreira, E. M.; Day, M. W. *Angew. Chem., Int. Ed.* **1997**, *36*, 1645−1647. (e) Jepsen, A. S.; Roberson, M.; Hazell, R. G.; Jørgensen, K. A. *Chem. Commun.* **1998**, 1599−1600. (f) Chang, C. J.; Connick, W. B.; Low, D. W.; Day, M. W.; Gray, H. B. *Inorg. Chem.* **1998**, *3*, 3107−3110. Mn nitrides with

cyclic amine donor ligands: (g) Niemann, A.; Bossek, U.; Haselhorst, G.; Wieghardt, K.; Nuber, B. *Inorg. Chem.* **1996**, *35*, 906–915. (h) Meyer, K.; Bendix, J.; Metzler-Nolte, N.; Weyhermueller, T.; Wieghardt, K. *J. Am. Chem. Soc.* **1998**, *120*, 7260–7270. (i) Grapperhaus, C. A.; Bill, E.; Weyhermueller, T.; Wieghardt, K. *Inorg. Chem.* **2001**, *40*, 4191–4198.

(4) (a) Grapperhaus, C. A.; Mienert, B.; Bill, E.; Weyhermueller, T.; Wieghardt, K. *Inorg. Chem.* **2000**, *39*, 5306–5317. (b) Betley, T. A.; Peters, J. C. *J. Am. Chem. Soc.* **2004**, *126*, 6252–6254. (c) Rohde, J.-U.; Betley, T. A.; Jackson, T. A.; Saouma, C. T.; Peters, J. C.; Que, L. *Inorg. Chem.* **2007**, *46*, 5720–5726.

(5) Ballhausen, C. J.; Gray, H. B. *Inorg. Chem.* **1962**, *1*, 111–122.

(6) Birk, T.; Bendix, J. *Inorg. Chem.* **2003**, *42*, 7608–7615.

(7) (a) For a previously crystallographically characterized Mn^{VII} nitride in an approximate C_{3v} environment, see: Danopoulos, A. A.; Wilkinson, G.; Sweet, T. K. N.; Hursthouse, M. B. *J. Chem. Soc., Dalton Trans.* **1995**, 205–216. (b) For an example of a Mn^V nitride within a cubane that is in an approximate C_{3v} environment, see: Vaddypally, S.; Kondaveeti, S. K.; Zdilla, M. J. *Inorg. Chem.* **2012**, *51*, 3950–3952.

(8) Parsell, T. H.; Behan, R. K.; Green, M. T.; Hendrich, M. P.; Borovik, A. S. *J. Am. Chem. Soc.* **2006**, *128*, 8728–8729.

(9) (a) Brown, S. D.; Betley, T. A.; Peters, J. C. *J. Am. Chem. Soc.* **2003**, *125*, 322–323. (b) Brown, S. D.; Peters, J. C. *J. Am. Chem. Soc.* **2005**, *127*, 1913–1923. (c) Thomas, C. M.; Mankad, N. P.; Peters, J. C. *J. Am. Chem. Soc.* **2006**, *128*, 4956–4957. (d) Moret, M.-E.; Peters, J. C. *Angew. Chem., Int. Ed.* **2012**, *50*, 2063–2067.

(10) Lu, C. C.; Peters, J. C. *Inorg. Chem.* **2006**, *45*, 8597–8607.

(11) A search of the CSD reveals that the (*N,N′*-bis(4,6-di-t-butylsalicylidene)-1,2-cyclohexanediaminato)-nitrido-manganese complex has a measured Mn–N bond distance of 1.561 Å: Ho, C.-M.; Lau, T.-C.; Kwong, H.-L.; Wong, W.-T. *J. Chem. Soc., Dalton Trans.* **1999**, 2411–2414.

(12) Berry, J. F.; Bill, E.; Bothe, E.; DeBeer George, S.; Mienert, B.; Neese, F.; Wieghardt, K. *Science* **2006**, *312*, 1937–1941.

(13) DeBeer George, S.; Petrenko, T.; Neese, F. *J. Phys. Chem. A* **2008**, *112*, 12936–12943.

(14) Glatzel, P.; Bergmann, U. *Coord. Chem. Rev.* **2005**, *249*, 65–95.

(15) Pollock, C. J.; DeBeer, S. *J. Am. Chem. Soc.* **2011**, *133*, 5594–5601.

(16) Delgado-Jaime, M. U.; Dible, B. R.; Chiang, K. P.; Brennessel, W. W.; Bergmann, U.; Holland, P. L.; DeBeer, S. *Inorg. Chem.* **2011**, *50*, 10709–10717.

(17) Lee, N.; Petrenko, T.; Bergmann, U.; Neese, F.; DeBeer, S. *J. Am. Chem. Soc.* **2010**, *132*, 9715–9727.

(18) (a) Groves, J. T.; Tadashi, T. *J. Am. Chem. Soc.* **1983**, *105*, 2074–2075. (b) Du Bois, J.; Tomooka, C. S.; Hong, J.; Carreira, E. M. *Acc. Chem. Res.* **1997**, *30*, 364–372.

(19) (a) Scepaniak, J. J.; Young, J. A.; Bontchev, R. P.; Smith, J. M. *Angew. Chem., Int. Ed.* **2009**, *48*, 3158–3160. (b) Scepaniak, J. J.; Bontchev, R. P.; Johnson, D. L.; Smith, J. M. *Angew. Chem., Int. Ed.* **2011**, *50*, 6630–6633. (c) Scepaniak, J. J.; Margarit, C. G.; Harvey, J. N.; Smith, J. M. *Inorg. Chem.* **2011**, *50*, 9508–9517.

(20) (a) Davies, H. M. L.; Manning, J. R. *Nature* **2008**, *451*, 417–424 and references therein. (b) Shaik, S.; Hirao, H.; Kumar, D. *Acc. Chem. Res.* **2007**, *40*, 532–542 and references therein.

15544

dx.doi.org/10.1021/ja306647c | *J. Am. Chem. Soc.* 2012, 134, 15538–15544